Advances in Nano Research, *Vol. 15, No. 2 (2023) 141-153*
https://doi.org/10.12989/anr.2023.15.2.141

Nonlinear finite element vibration analysis of functionally graded nanocomposite spherical shells reinforced with graphene platelets

Xiaojun Wu*

Institute of Automobile Engineering, Chongqing Industry Polytechnic College, Chongqing 401120, Chongqing, China

(*Received June 22, 2022, Revised February 26, 2023, Accepted March 13, 2023*)

Abstract. The main objective of this paper is to develop the finite element study on the nonlinear free vibration of functionally graded nanocomposite spherical shells reinforced with graphene platelets under the first-order shear deformation shell theory and von Kármán nonlinear kinematic relations. The governing equations are presented by introducing the full asymmetric nonlinear strain-displacement relations followed by the constitutive relations and energy functional. The extended Halpin-Tsai model is utilized to specify the overall Young's modulus of the nanocomposite. Then, the finite element formulation is derived and the quadrilateral 8-node shell element is implemented for finite element discretization. The nonlinear sets of dynamic equations are solved by the use of the harmonic balance technique and iterative method to find the nonlinear frequency response. Several numerical examples are represented to highlight the impact of involved factors on the large-amplitude vibration responses of nanocomposite spherical shells. One of the main findings is that for some geometrical and material parameters, the fundamental vibrational mode shape is asymmetric and the axisymmetric formulation cannot be appropriately employed to model the nonlinear dynamic behavior of nanocomposite spherical shells.

Keywords: functionally graded graphene platelet reinforced composite; nanocomposite spherical shell; nonlinear finite element analysis; nonlinear vibration; shear deformation shell theory

1. Introduction

Due to the advancements in manufacturing technologies and demands for lightweight structures in several engineering fields such as aerospace, automobile, and marine industries, nanocomposite structures have received considerable attention among research communities. Functionally graded nanocomposites (FGNC) reinforced with carbon nanotubes or graphene platelets (GPLs) are recently introduced as lightweight advanced polymer-based nanocomposites with great potential in several industrial applications following their mechanical characteristics such as high strength-to-weight ratio.

The linear static and dynamic structural mechanics of FGNC beam (Nejadi *et al*. 2021), plate (Shen *et al*. 2017a, Song *et al*. 2018, Yang *et al*. 2018, Ebrahimi and Habibi 2017, Kumar *et al*. 2021, Khadir *et al*. 2021), panel (Salami *et al*. 2021), and shell (Hajmohammad *et al*. 2018, Liu *et al*. 2018, Kiarasi *et al*. 2021, Qin *et al*. 2020, Kiani 2019) structures have been widely studied to highlight the novel structural aspects of nanocomposites showing the importance of these members in engineering technologies. In this topical area, some investigations on the mechanics of FGNC plates and shells were performed by Kitipornchai and his colleagues (Song *et al*. 2018, Yang *et al*. 2018, Liu *et al*. 2018) using the analytical solution method. The Gram-Schmidt-based analytical solution for linear vibration of FGNC shallow shells was also developed by Qin *et al*. (2020). In addition, Kiani (2019) outlined the thermo-mechanical buckling analysis of nanocomposite conical shells by developing the semi-analytical solution using the generalized differential quadrature (GDQ) and Fourier expansion. A detailed review article has been recently published by Zhao *et al*. (2020) on the mechanics of FGNC structures reinforced with GPLs which can provide comprehensive details for interested readers.

On the other hand, the applications of numerical simulation methods in the structural analysis have been expanded in the past two decades. Tornabene *et al*. (2012) conducted a study based on the GDQ method on linear free vibration of doubly-curved shells and panels with a free-form meridian. Fantuzzi *et al*. (2014) extended the applications of the GDQ method for arbitrarily shaped membranes. By applying the numerical solution strategy based on the transformed differential quadrature method and a multi-step time integration scheme under a NURBS interpolation, Heydarpor *et al*. (2020) simulated the linear thermoelastic behavior of rotating multilayer FGNC conical shells. The meshfree radial point interpolation method has been also employed by Noroozi *et al*. (2020) to investigate the vibration and buckling of FGNC perforated plates subjected to the in-plane loadings. Also, related to this study, several numerical studies on vibrational analysis of coupled circular nanocomposite shells have been performed in the literature following different shell models using the GDQ-based solution methods (Sobhani 2022, 2023a, b, Sobhani and Avcar 2022a, b, Sobhani and Masoodi 2022, Sobhani *et al*. 2022a, b, c, 2023a). For instance, Sobhani *et al*. (2022a) studied the free-damped vibration of FGNC coupled conical-cylindrical shell structures. Also, the dynaamics of joined sandwich nanocomposite spherical-

*Corresponding author, Ph.D.,
E-mail: zzbizwu@163.com

ISSN: 2287-237X (Print), 2287-2388 (Online)

conical shells subjected to spring boundary conditions was investigated by Sobhani (2023a).

Unlike the vast range of linear analyses, much fewer studies focused on the nonlinear mechanical behavior of FGNCs due to the more complex nature of governing equations. For instance, using a perturbation-based analytical method and under Reddy's shell model, Shen *et al*. (2017b, c) presented various studies on the nonlinear dynamic and postbuckling of nanocomposite plates and cylindrical shells reinforced with FG graphenes. In addition, Gao *et al*. (2018) investigated the effects of the elastic medium on the large-amplitude dynamics of porous FGNC plates following the thin plate theory and geometric nonlinearity using the differential quadrature (DQ) technique. The nonlinear dynamic analysis of FGNC conical shells reinforced with graphenes was also demonstrated by Wang *et al*. (2019) under the shear deformation model applying the Galerkin method and the fourth-order Runge–Kutta technique. Besides, several numerical methods such as the DQ method (Gholami and Ansari 2018), element-free approach (Selim and Liu 2021), singular convolution technique (Civalek 2020), and finite element method have been recently applied to perform numerical studies on the structural mechanics of FGNCs. To get more details, one can consider the review study by Zhao *et al*. (2020).

On the other hand, in comparison to the wide range of studies on the mechanical analysis of FGNC structures, limited works have been published on nanocomposite spherical shells. The linear vibration of FGNC spherical shells reinforced with CNTs resting on the elastic medium was investigated by Ansari *et al*. (2016, 2020) using the DQ numerical solution method. The Rayleigh-Ritz analytical solution based on the improved Fourier series admissible functions was developed by Wang *et al*. (2018) to focus on the vibration analysis of FGNC spherical panels and shells reinforced with CNTs with general elastic restraints. Also, the vibration analysis of CNT-FGNC spherical caps was analyzed by Kiani (2017) under the shear deformation formulation using the Ritz method and Gram-Schmidt process. On the other hand, regarding the studies for GPL-reinforced nanocomposite, the isogeometric analysis method was employed to study the static and dynamic analysis of FGNC cylindrical and spherical panels (Van Do *et al*. 2020, Tao and Dai 2021). Following the 3D elasticity model and analytical solution method, Liu *et al* (2021) also dealt with the vibration and bending analysis of FGNC spheres. Recently, Haboussi *et al*. (2021) highlighted the nonlinear axisymmetric dynamic buckling of FGNC spherical caps in which the one-dimensional finite element analysis was performed under the axisymmetric formulation. Newmark's integration technique was employed to find the dynamic response.

As the survey of the literature indicates, a wide range of studies have been recently performed on the vibration analysis of nanocomposite shells and panels, however, most of the studies on complex geometries have been carried out on linear vibration analysis, and geometric nonlinearity has been less considered for nanocomposite shells and panels. In addition, to the best of the author's knowledge, the nonlinear vibration of functionally graded nanocomposite spherical shells reinforced with graphene platelets has not been addressed yet in the literature. Therefore, the main objective of this research is to develop an efficient finite element model to study the nonlinear free vibration of FGNC spherical shells reinforced with GPLs. Since the fundamental vibrational mode shape is not axisymmetric for some geometrical parameters, the full asymmetric formulation under the shear deformation theory is presented where von Kármán's geometrically nonlinear assumption is regarded. The extended Halpin-Tsai model is followed to give the effective elasticity modulus. The nonlinear strain-displacement approach and constitutive relations are presented to form the energy functional of the system and the 8-node quadrilateral shell elements in the spherical coordinate system are employed for finite element discretization. The nonlinear sets of algebraic governing equations are finally solved using the modified Newton-Raphson iteration technique and the Harmonic method to give the nonlinear vibration response. Several numerical examples are represented to highlight the impacts of geometrical parameters, nanocomposite materials, and boundary conditions of the vibration characteristics of functionally graded GPL-reinforced nanocomposite spherical shells.

2. Functionally graded nanocomposite

The effective material properties of the FGNC are described in this section. It is assumed that the spherical shell is made of an epoxy-based composite material reinforced by GPLs. The extended Halpin-Tsai (EHT) model is utilized to estimate the overall elastic modulus of the FGNC in which the influences of GPL dimensions on the material properties are accounted. Following the EHT model, Young's modulus of the FGNC reinforced by GPLs is given by (Song *et al*. 2018)

$$E = \frac{3}{8}\left(\frac{1+\xi_L\eta_L V_{gpl}}{1-\eta_L V_{gpl}}\right)E_m + \frac{5}{8}\left(\frac{1+\xi_W\eta_W V_{gpl}}{1-\eta_W V_{gpl}}\right)E_m \quad (1)$$

with

$$\eta_L = \frac{(E_{gpl}/E_m)-1}{(E_{gpl}/E_m)-\xi_L}, \qquad \eta_W = \frac{(E_{gpl}/E_m)-1}{(E_{gpl}/E_m)-\xi_W} \quad (2)$$

where $\xi_L = 2(l_{gpl}/h_{gpl})$ and $\xi_W = 2(w_{gpl}/h_{gpl})$ are the geometrical factors defined for the GPL. Additionally, the mass density and Poisson's ratio of FGNC are

$$\begin{aligned} \rho &= V_{gpl}\rho_{gpl} + V_M\rho_m, \\ \nu &= V_{gpl}\nu_{gpl} + V_m\nu_m \end{aligned} \quad (3)$$

In the above equations $E, V, \rho,$ and ν stand for the elastic modulus, volume fraction, mass density, and Poisson's ratio, respectively where the subscripts gpl and m denote the corresponding properties for GPL and matrix phase of the nanocomposite.

To improve the structural vibration performance of the shell, the uniform distribution (UD) or functionally graded patterns (like FG-A, FG-O, and FG-X shown in Fig. 1) of

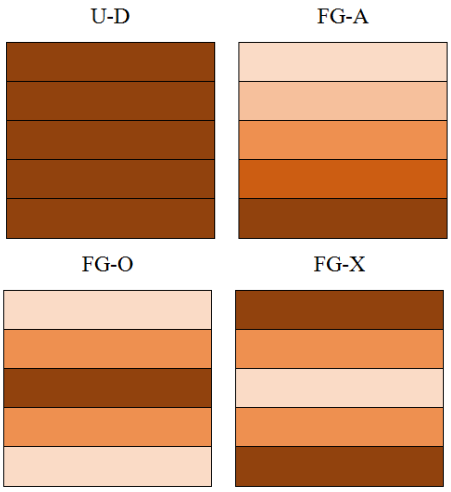

Fig. 1 The dispersion patterns of GPLs through the thickness of the FG-NC spherical shell

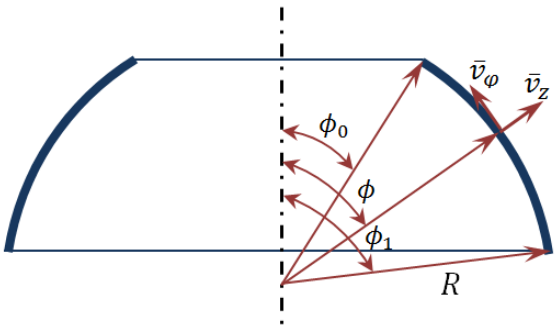

Fig. 2 Schematic view and geometrical parameters of the spherical shell

GPs through the thickness direction are considered. From the mathematical point of view, the GPLs' volume fraction for each case is expressed as follows

$$\begin{aligned} \text{UD:}\quad & V_{gpl} = V_{gpl}^* \\ \text{FG-A:}\quad & V_{gpl} = \left(1-\frac{2z}{h}\right)V_{gpl}^* \\ \text{FG-O:}\quad & V_{gpl} = 2\left(1-\frac{2|z|}{h}\right)V_{gpl}^* \\ \text{FG-X:}\quad & W_{gpl} = 2\left(\frac{2|z|}{h}\right)V_{gpl}^* \end{aligned} \tag{4}$$

in which h signifies the plate thickness and

$$V_{gpl}^* = \frac{W_{gpl}^*}{W_{gpl}^* + \frac{\rho_{gpl}}{\rho_M}\left(1-W_{gpl}^*\right)} \tag{5}$$

is GPLs total volume fraction.

3. Fundamental equations

The spherical shell which is shown in Fig. 2 with radius R, meridional angles φ_1 and φ_2 and thickness h is considered in this study. The governing equations including the geometrically nonlinear kinematic relations, constitutive relations, and the energy functional are presented in this section under the first-order shear deformation shell theory (FSDST) and von Kármán assumptions following the asymmetric formulation in the spherical coordinate system of φ, θ, z. By taking $v_i\ (i = \varphi, \theta, z)$ as the mid-surface displacements and ψ_φ, ψ_θ as the rotations into consideration under the FSDST, the displacement field is

$$\begin{aligned} \bar{v}_\varphi &= v_\varphi(\varphi,\theta) + z\psi_\varphi(\varphi,\theta), \\ \bar{v}_\theta &= v_\theta(\varphi,\theta) + z\psi_\theta(\varphi,\theta), \\ \bar{v}_z &= v_z(\varphi,\theta) \end{aligned} \tag{6}$$

On the basis of the Donnell shell model and the von Kármán nonlinear kinematics, the strain vectors are defined as (Tornabene and Viola 2007)

$$\boldsymbol{\epsilon} = \begin{Bmatrix} \epsilon_\varphi \\ \epsilon_\theta \\ \gamma_{\varphi\theta} \end{Bmatrix} = \boldsymbol{\epsilon}_m + z\boldsymbol{\epsilon}_b + \boldsymbol{\epsilon}_{nl}, \quad \boldsymbol{\epsilon}_s = \begin{Bmatrix} \gamma_{\theta z} \\ \gamma_{\varphi z} \end{Bmatrix} \tag{7}$$

in which

$$\boldsymbol{\epsilon}_m = \begin{Bmatrix} \frac{1}{R}\left(v_{\varphi,\varphi} + v_z\right) \\ \frac{v_{\theta,\theta}}{\sin\varphi} + \frac{v_\varphi}{\tan\varphi} + \frac{v_z}{R} \\ \frac{v_{\theta,\phi}}{R} + \frac{v_{\varphi,\theta}}{\sin\varphi} - \frac{v_\theta}{\tan\varphi} \end{Bmatrix},$$

$$\boldsymbol{\epsilon}_b = \begin{Bmatrix} \frac{\psi_{\varphi,\varphi}}{R} \\ \frac{\psi_{\theta,\theta}}{\sin\varphi} + \frac{\psi_\varphi}{\tan\varphi} \\ \frac{\psi_{\theta,\varphi}}{R} + \frac{\psi_{\varphi,\theta}}{\sin\varphi} - \frac{\psi_\theta}{\tan\varphi} \end{Bmatrix}, \tag{8}$$

$$\boldsymbol{\epsilon}_{nl} = \frac{1}{2}\begin{Bmatrix} \frac{v_{z,\varphi}v_{z,\varphi}}{R^2} \\ \frac{v_{z,\theta}v_{z,\theta}}{\sin^2\varphi} \\ \frac{2}{R}\frac{v_{z,\varphi}v_{z,\theta}}{\sin\varphi} \end{Bmatrix}, \qquad \boldsymbol{\epsilon}_s = \begin{Bmatrix} \psi_\varphi + \frac{v_{z,\phi}}{R} - \frac{v_\varphi}{R} \\ \psi_\theta + \frac{v_{z,\theta}}{\sin\varphi} - \frac{v_\theta}{R} \end{Bmatrix}$$

where $\boldsymbol{\epsilon}_m, \boldsymbol{\epsilon}_b, \boldsymbol{\epsilon}_s$ are the linear membrane, bending, and transverse shear strains while $\boldsymbol{\epsilon}_{nl}$ signifies the impact of the geometrically nonlinear assumptions. Note that comma (",") symbolizes the derivative operator, for example, we have $v_{\varphi,\varphi} = \frac{\partial v_\varphi}{\partial \varphi}$. Based on the defined effective material properties in section 2 and under the linear elastic material assumption, the stress vectors can be given by

$$\begin{aligned} \boldsymbol{\sigma} &= \begin{Bmatrix} \sigma_\varphi \\ \sigma_\theta \\ \sigma_{\varphi\theta} \end{Bmatrix} = \begin{bmatrix} Q_{11}(z) & Q_{12}(z) & 0 \\ Q_{12}(z) & Q_{22}(z) & 0 \\ 0 & 0 & Q_{66}(z) \end{bmatrix} \begin{Bmatrix} \epsilon_\varphi \\ \epsilon_\theta \\ \gamma_{\varphi\theta} \end{Bmatrix} = \boldsymbol{Q}\boldsymbol{\epsilon}, \\ \boldsymbol{\sigma}^s &= \begin{Bmatrix} \sigma_{\theta z} \\ \sigma_{\varphi z} \end{Bmatrix} = \begin{bmatrix} Q_{44} & 0 \\ 0 & Q_{55} \end{bmatrix} \begin{Bmatrix} \gamma_{\theta z} \\ \gamma_{\varphi z} \end{Bmatrix} = \boldsymbol{Q}^s\boldsymbol{\epsilon}_s \end{aligned} \tag{9}$$

where

$$\begin{aligned} Q_{11}(z) &= \frac{E(z)}{1-\nu^2(z)}, \qquad Q_{22} = Q_{11}, \\ Q_{12}(z) &= \frac{E(z)\nu(z)}{1-\nu^2(z)}, \\ Q_{66}(z) &= \frac{E(z)}{2[1+\nu(z)]}, \qquad Q_{55} = Q_{44} = Q_{66} \end{aligned} \tag{10}$$

Taking this point into account that the formulation is given by the FSDST, the stress resultants are expressed by integrating the stresses over the thickness direction

$$\begin{Bmatrix}\mathbf{P}\\ \mathbf{M}\\ \mathbf{T}\end{Bmatrix}=\begin{bmatrix}\boldsymbol{\mathcal{A}} & \boldsymbol{\mathcal{B}} & \mathbf{0}\\ \boldsymbol{\mathcal{B}} & \boldsymbol{\mathcal{D}} & \mathbf{0}\\ \mathbf{0} & \mathbf{0} & \kappa_s\boldsymbol{\mathcal{A}}^s\end{bmatrix}\left(\begin{Bmatrix}\boldsymbol{\epsilon}_m\\ \boldsymbol{\epsilon}_b\\ \boldsymbol{\epsilon}_s\end{Bmatrix}+\frac{1}{2}\begin{Bmatrix}\boldsymbol{\epsilon}_{nl}\\ \mathbf{0}\\ \mathbf{0}\end{Bmatrix}\right)=\widehat{\boldsymbol{\mathcal{D}}}\left(\hat{\boldsymbol{\epsilon}}+\frac{1}{2}\hat{\boldsymbol{\epsilon}}_{nl}\right), \tag{11}$$

in which

$$\hat{\boldsymbol{\epsilon}}=\begin{Bmatrix}\boldsymbol{\epsilon}_m\\ \boldsymbol{\epsilon}_b\\ \boldsymbol{\epsilon}_s\end{Bmatrix},\qquad \hat{\boldsymbol{\epsilon}}_{nl}=\begin{Bmatrix}\boldsymbol{\epsilon}_{nl}\\ \mathbf{0}\\ \mathbf{0}\end{Bmatrix} \tag{12}$$

where κ_s is the shear correction factor. Note that within the first-order shear deformation theory, the shear correction factor is determined following the exact stress distribution through the thickness by comparing the strain energy due to the 3D elasticity theory and first-order shear deformation theory. However, because of the difficulties in 3D elasticity analyses, the approximate value of the shear correction factor factor κ_s=5/6 is commonly used for composite plates and shells. Hence, in this research, the same value has been considered for the shear correction factor. Also, $\mathbf{P}=\{P_\varphi\ P_\theta\ P_{\varphi\theta}\}^{\mathrm{T}}$ is the vector of force resultant, $\mathbf{M}=\{M_\varphi\ M_\theta\ M_{\varphi\theta}\}^{\mathrm{T}}$ is the vector of moment resultants, and $\mathbf{T}=\{T_{\theta z}\ N_{\varphi z}\}^{\mathrm{T}}$ is the vector of shear force resultant and

$$(\boldsymbol{\mathcal{A}}_{3\times3},\boldsymbol{\mathcal{B}}_{3\times3},\boldsymbol{\mathcal{D}}_{3\times3})=\int_{-h/2}^{h/2}\boldsymbol{\mathcal{Q}}(1,z,z^2)dz,\qquad \boldsymbol{\mathcal{A}}^s_{2\times2}=\int_{-h/2}^{h/2}\boldsymbol{\mathcal{Q}}^s dz \tag{13}$$

Hamilton's principle is used in this study to derive the finite element formulation. In this regard, the energy functional of the system needs to be presented first. By the use of kinematic and constitutive relations, the variation of strain energy of the FGNC spherical shell can be expressed as

$$\delta\mathcal{U}=\int_\Omega\delta\left(\hat{\boldsymbol{\epsilon}}+\frac{1}{2}\hat{\boldsymbol{\epsilon}}_{nl}\right)^{\mathrm{T}}\widehat{\boldsymbol{\mathcal{D}}}\left(\hat{\boldsymbol{\epsilon}}+\frac{1}{2}\hat{\boldsymbol{\epsilon}}_{nl}\right)d\Omega \tag{14}$$

Also, by introducing the displacement field in the matrix form like

$$\boldsymbol{v}=\begin{bmatrix}\bar{v}_\varphi\\ \bar{v}_\theta\\ \bar{v}_z\end{bmatrix}=\mathbf{P_0}\boldsymbol{\mathcal{V}},\qquad \mathbf{P}_0=\begin{bmatrix}1&0&0&z&0\\0&1&0&0&z\\0&0&1&0&0\end{bmatrix},\qquad \boldsymbol{\mathcal{V}}=[v_\varphi\quad v_\theta\quad v_z\quad \psi_\varphi\quad \psi_\theta\,]^{\mathrm{T}} \tag{15}$$

the first variation of the kinetic energy will be

$$\delta\mathcal{K}=\int_V\delta\boldsymbol{v}^{\mathrm{T}}\rho\,\ddot{\boldsymbol{v}}\,dV=\int_\Omega\delta\boldsymbol{\mathcal{V}}^{\mathrm{T}}\mathfrak{M}\,\ddot{\boldsymbol{\mathcal{V}}}\,d\Omega \tag{16}$$

in which

$$\mathfrak{M}=\int_{-\frac{h}{2}}^{\frac{h}{2}}\mathbf{P}_0^{\mathrm{T}}\rho\mathbf{P}_0dz \tag{17}$$

In addition, the variation of the work of the external loads is

$$\delta\mathcal{W}=\int_\Omega\delta\boldsymbol{\mathcal{V}}^{\mathrm{T}}\mathbf{f}\,d\Omega \tag{18}$$

where by considering the shell subjected to the uniformly distributed radial load (f), we have $\mathbf{f}=[0\ 0\ 0\ 0\ f]^{\mathrm{T}}$.

Finally, with the aid of strain energy (Eq. 14), kinematic energy (Eq. 16), and work of external forces (Eq. 18), Hamilton's principle can be expressed as

$$\int_{t_1}^{t_2}\left\{\int_\Omega\delta\left(\hat{\boldsymbol{\epsilon}}+\frac{1}{2}\hat{\boldsymbol{\epsilon}}_{nl}\right)^{\mathrm{T}}\widehat{\boldsymbol{\mathcal{D}}}\left(\hat{\boldsymbol{\epsilon}}+\frac{1}{2}\hat{\boldsymbol{\epsilon}}_{nl}\right)+\int_\Omega\delta\boldsymbol{\mathcal{V}}^{\mathrm{T}}\mathfrak{M}\,\ddot{\boldsymbol{\mathcal{V}}}\,d\Omega-\int_\Omega\delta\boldsymbol{\mathcal{V}}^{\mathrm{T}}\mathbf{f}\,d\Omega\right\}dt=0 \tag{19}$$

4. Finite element analysis

The finite element procedure for nonlinear vibration of the FGNC spherical shell is formulated in this section. The eight-node shell element defined in the local spherical coordinate of x,y (corresponds to the global coordinates of φ,θ) is considered here for the FE discretization with the following shape functions

$$\begin{aligned}N_1&=-\frac{1}{4}(1-x)(1-y)(1+x+y),\\ N_5&=\frac{1}{2}(1-x^2)(1-y)\\ N_2&=-\frac{1}{4}(1+x)(1-y)(1-x+y),\\ N_6&=\frac{1}{2}(1+x)(1-y^2)\\ N_3&=-\frac{1}{4}(1+x)(1+y)(1-x-y),\\ N_7&=\frac{1}{2}(1-x^2)(1+y)\\ N_4&=-\frac{1}{4}(1-x)(1-y)(1+x-y),\\ N_8&=\frac{1}{2}(1-x)(1-y^2)\end{aligned} \tag{20}$$

Accordingly, the displacement vector $\boldsymbol{\mathcal{V}}$ defined in Eq. 15 can be approximated by

$$\boldsymbol{\mathcal{V}}=\sum_{i=1}^{8}\mathbf{N}^i\,\mathbf{q}^i=\mathbf{N}\mathbf{q} \tag{21}$$

$$\mathbf{N}=[\mathbf{N}^1\ \mathbf{N}^2\ \ldots\ \mathbf{N}^8],\qquad \mathbf{N}^i=\begin{bmatrix}N_i&0&0&0&0\\ &N_i&0&0&0\\ &&N_i&0&0\\ &&&N_i&0\\ \mathrm{sym}&&&&N_i\end{bmatrix} \tag{22}$$

where we have $\mathbf{q}=[\mathbf{q}^1\ \mathbf{q}^2\ \ldots\ \mathbf{q}^8]^{\mathrm{T}}$ in which $\mathbf{q}^i=\left[v_\varphi^i\quad v_\theta^i\quad v_z^i\quad \psi_\varphi^i\quad \psi_\theta^i\right]^{\mathrm{T}}$ is the vector of unknown nodal values at each node within an element. Now, by substituting the approximation of the displacement vector from Eq. (21) into linear and nonlinear strains of Eq. (12), the strains can be approximated by

$$\hat{\boldsymbol{\epsilon}} = \begin{Bmatrix} \boldsymbol{\epsilon}_m \\ \boldsymbol{\epsilon}_b \\ \boldsymbol{\epsilon}_s \end{Bmatrix} = \sum_{i=1}^{8} \begin{Bmatrix} \boldsymbol{\mathcal{B}}_m \\ \boldsymbol{\mathcal{B}}_b \\ \boldsymbol{\mathcal{B}}_s \end{Bmatrix}^i \mathbf{q}^i = \boldsymbol{\mathcal{B}}\mathbf{q}, \qquad \boldsymbol{\epsilon}_{nl} = \sum_{i=1}^{8} \boldsymbol{\Theta}^i \boldsymbol{\mathcal{B}}_{nl}^i \mathbf{q}^i = \boldsymbol{\mathcal{B}}_{nl}\mathbf{q}, \tag{23}$$

where by recalling the strain components in Eq. (8) we have

$$\boldsymbol{\mathcal{B}}_m^i = \begin{bmatrix} \frac{N_{i,\varphi}}{R} & 0 & \frac{N_i}{R} & 0 & 0 \\ \frac{N_i}{\tan\varphi_i} & \frac{N_{i,\theta}}{\sin\varphi_i} & \frac{N_i}{R} & 0 & 0 \\ \frac{N_{i,\theta}}{\sin\varphi_i} & \frac{N_{i,\varphi}}{R} - \frac{N_i}{\tan\varphi_i} & 0 & 0 & 0 \end{bmatrix} \tag{24}$$

$$\boldsymbol{\mathcal{B}}_b^i = \begin{bmatrix} 0 & 0 & 0 & \frac{N_{i,\varphi}}{R} & 0 \\ 0 & 0 & 0 & \frac{N_i}{\tan\varphi_i} & \frac{N_{i,\theta}}{\sin\varphi_i} \\ 0 & 0 & 0 & \frac{N_{i,\theta}}{\sin\varphi_i} & \frac{N_{i,\varphi}}{R} - \frac{N_i}{\tan\varphi_i} \end{bmatrix}, \tag{25}$$

$$\boldsymbol{\mathcal{B}}_s^i = \begin{bmatrix} -\frac{N_i}{R} & 0 & \frac{N_{i,\varphi}}{R} & N_i & 0 \\ 0 & -\frac{N_i}{R} & \frac{N_{i,\theta}}{\sin\varphi_i} & 0 & N_i \end{bmatrix},$$

$$\boldsymbol{\Theta}^i = \begin{bmatrix} \frac{v_{z,\varphi}^i}{R} & 0 \\ 0 & \frac{v_{z,\theta}^i}{\sin\varphi_i} \\ \frac{v_{z,\theta}^i}{\sin\varphi_i} & \frac{v_{z,\varphi}^i}{R} \end{bmatrix}, \qquad \boldsymbol{\mathcal{B}}_{nl}^i = \begin{bmatrix} 0 & 0 & \frac{N_{i,\varphi}}{R} & 0 & 0 \\ 0 & 0 & \frac{N_{i,\theta}}{\sin\varphi_i} & 0 & 0 \end{bmatrix}, \tag{26}$$

Next, by substituting Eq. (21) and Eq. (23) into Hamilton's principle, it can be written

$$\int_{t_1}^{t_2} \Big\{ \int_\Omega \delta\mathbf{q}^{\mathrm{T}} \Big(\boldsymbol{\mathcal{B}}^{\mathrm{T}} \widehat{\boldsymbol{\mathcal{D}}} \boldsymbol{\mathcal{B}} + \tfrac{1}{2} \boldsymbol{\mathcal{B}}^{\mathrm{T}} \widehat{\boldsymbol{\mathcal{D}}} \boldsymbol{\mathcal{B}}_{nl} + \boldsymbol{\mathcal{B}}_{nl}^{\mathrm{T}} \widehat{\boldsymbol{\mathcal{D}}} \boldsymbol{\mathcal{B}} + \tfrac{1}{2} \boldsymbol{\mathcal{B}}_{nl}^{\mathrm{T}} \widehat{\boldsymbol{\mathcal{D}}} \boldsymbol{\mathcal{B}}_{nl} \Big) \mathbf{q} \, d\Omega + \int_\Omega \delta\mathbf{q}^{\mathrm{T}} \mathbf{N}^{\mathrm{T}} \mathfrak{M} \mathbf{N} \ddot{\mathbf{q}} \, d\Omega - \int_\Omega \delta\mathbf{q}^{\mathrm{T}} \mathbf{N}\mathbf{f} \, d\Omega \Big\} dt = 0 \tag{27}$$

This leads to the following nonlinear sets of FE formulation for nonlinear vibration of FGNC spherical shell

$$\mathbf{M}\ddot{\mathbf{q}} + \mathbf{K}(\mathbf{q})\mathbf{q} = \mathbf{F} \tag{28}$$

with the following stiffness matrices

$$\mathbf{K} = \mathbf{K}_{\text{linear}} + \mathbf{K}_{\text{nonlinear}}$$

$$\mathbf{K}_{\text{linear}} = \int_\Omega \boldsymbol{\mathcal{B}}^{\mathrm{T}} \widehat{\boldsymbol{\mathcal{D}}} \boldsymbol{\mathcal{B}} \, d\Omega, \tag{29}$$

$$\mathbf{K}_{\text{nonlinear}} = \int_\Omega \Big(\frac{1}{2} \boldsymbol{\mathcal{B}}^{\mathrm{T}} \widehat{\boldsymbol{\mathcal{D}}} \boldsymbol{\mathcal{B}}_{nl} + \boldsymbol{\mathcal{B}}_{nl}^{\mathrm{T}} \widehat{\boldsymbol{\mathcal{D}}} \boldsymbol{\mathcal{B}} + \frac{1}{2} \boldsymbol{\mathcal{B}}_{nl}^{\mathrm{T}} \widehat{\boldsymbol{\mathcal{D}}} \boldsymbol{\mathcal{B}}_{nl} \Big) \, d\Omega,$$

and the mass matrix as well as the force vector

$$\mathbf{M} = \int_\Omega \mathbf{N}^{\mathrm{T}} \mathfrak{M} \mathbf{N} \, d\Omega, \tag{30}$$

$$\mathbf{F} = \int_\Omega \mathbf{N}^{\mathrm{T}} \mathbf{f} \, d\Omega \tag{31}$$

The Gauss quadrature integration scheme is used to calculate the stiffness and mass matrices as well as the force vector. The reduced integration approach is also applied to avoid the shear locking phenomenon.

As one of the practical techniques for solving large-amplitude dynamic problems, the harmonic balance method (HBM) is employed in this study. The Fourier series is utilized to propose a regular periodic response for an ordinary differential equation system (Krack and Gross 2019). On the basis of the HBM and by considering the periodic response $\mathbf{q}(t) = \mathbf{q}(t+T)$ with $T = 2\pi/\omega$, the unknown vector $\mathbf{q}$ is introduced with the following ansatz (Krack and Gross 2019)

$$\mathbf{q}_h(t) = \mathbf{X}_0 + \sum_{p=1}^{\infty} \mathbf{X}_{s,p} \sin(p\omega t) + \sum_{p=1}^{\infty} \mathbf{X}_{c,p} \cos(p\omega t) = \Re\left\{ \sum_{p=0}^{\infty} \mathbf{X}_p \mathrm{e}^{(ip\omega t)} \right\} \tag{32}$$

with i as the imaginary number and $\Re$ for the real part of the relation. Next, we have

$$\mathbf{q}_h = \Re\left\{ \sum_{p=0}^{\infty} \mathbf{X}_p \mathrm{e}^{(ip\omega t)} \right\}, \quad \ddot{\mathbf{q}}_h = \Re\left\{ \sum_{p=0}^{\infty} -(p\omega)^2 \mathbf{X}_p \mathrm{e}^{(ip\omega t)} \right\} \tag{33}$$

By setting Eq. (33) into Eq. (28), it can be written

$$\Re\left\{ \sum_{p=0}^{\infty} \big([-(p\omega)^2 \mathbf{M} + \mathbf{K}] \mathbf{X}_p - \mathbf{F} \big) \mathrm{e}^{(ip\omega t)} \right\} = \mathbf{R} \tag{34}$$

where $\mathbf{R}$ denotes the residual of the Fourier approximation. Finally, the weighted residual approach is applied and the residual $\mathbf{R}$ can be minimized by

$$\int_0^T \mathbf{R} \, \mathrm{e}^{(-ip\omega t)} dt = 0 \tag{35}$$

Eq. (35) gives the sets of nonlinear algebraic equations where iterative techniques like the Newton-Raphson method can be implemented to solve it and find the nonlinear vibration response.

5. Numerical examples

The FGNC is composed of the polymer matrix and GPLs with these geometrical dimensions: $l_{gpl} = 2.5\ \mu$m, $w_{gpl} = 1.5\ \mu$m and $h_{gpl} = 1.5$ nm as the reinforcement which is functionally graded along with the thickness of the spherical shell. The material properties are (Song *et al.* 2018):

Polymer matrix: $E_M = 3$ GPa, $\nu_M = 0.34$ and $\rho_M = 1.2$ g/cm^3

GPL reinforcement: $E_{gpl} = 1.01$ TPa, $\nu_{gpl} = 0.186$ *and* $\rho_{gpl} = 1.06 \frac{g}{cm^3}$

Two types of boundary support including the fixed (F) or clamped and hinged (H) or simply-supported are regarded at the edges of the shell with the following mathematical expressions:

$$\text{Fixed (F):}\ v_\varphi = v_\theta = v_z = \psi_\varphi = \psi_\theta = 0 \qquad \text{Hinged (H):}\ v_\varphi = v_\theta = v_z = 0 \tag{36}$$

Table 1 Comparative study for the natural frequencies $f = \omega_l/2\pi$ (Hz) of FG spherical shell

k	mode number	F-F		H-H	
		Present work	Qu et al. (2013)	Present work	Qu et al. (2013)
0.6	1	873.54	873.65	767.78	767.93
	2	888.03	888.18	815.03	815.16
	3	893.59	893.72	885.39	885.52
	4	908.41	908.59	887.68	887.89
5	1	862.49	862.63	749.66	749.86
	2	866.70	866.84	796.65	796.84
	3	869.91	870.03	863.08	863.22
	4	896.48	896.77	864.16	864.39
20	1	852.01	852.12	746.47	746.63
	2	855.55	855.73	790.52	790.75
	3	858.57	858.70	850.34	850.56
	4	885.62	885.80	852.39	852.64

Table 2 Comparison study for the natural frequencies (Hz) of the fixed-fixed isotropic semi-spherical shell

Mode number	F-F	
	Sobhani (2023b)	Present work
1	110.79	110.58
2	119.00	118.97
3	120.54	120.90
4	123.19	123.25
5	125.79	125.83

And to make the boundary supports' notation more clear, it should be pointed out that for instance, F-H denotes that the upper edge of the shell is fixed while the bottom edge is hinged.

To demonstrate the accuracy of the proposed FE analysis, three comparative examples with the results published in the open literature are represented first. For the first example, the natural frequencies of the FG shell are compared to the results given by Qu *et al*. (2013) in Table 1 for diverse FG power-law indexes and two boundary supports. The geometrical parameters of the shell are: $R = 1$ m, $R/h = 20, \varphi_0 = 15^\circ$, $\varphi_1 = 90^\circ$.

As the second comparative study, the first five natural frequencies (Hz) of the isotropic semi-spherical shell are compared in Table 2 for fixed-fixed (F-F) boundary conditions. The geometrical parameters are $R/h = 66.7$, $\phi_0 = 14.63^\circ$, $\phi_1 = 90^\circ$. Next, the comparison of the non-dimensional frequencies ($\widehat{\omega}_l = \omega_l R^2\sqrt{I_m/D_m}$) of FGNC spherical shells reinforced with CNTs are reported in Table 3 with the results given in Ansari *et al*. (2016). The dimensions of the shell are: $R/h = 50, \phi_0 = 15^\circ, \phi_1 = 90^\circ$. Note that $V^*_{cnt}$is the volume fraction of CNTs within the FGNC. The excellent agreements (less than 0.5% difference) between the results indicate the accuracy of the model.

The numerical efficiency of the FE analysis is further discussed in Fig. 3 for two radius to thickness ratios (RTRs) where the convergence of the frequency parameters of the FGNC spherical shell with Fixed-Fixed boundary supports. Note that in this study, the frequency parameter is defined as:

$$\bar{\omega}_l = \frac{\omega_l R^2}{\pi^2}\sqrt{I_m/D_m} \tag{37}$$

where $I_m = \rho_m h$, $D_m = D_m = \frac{E_m h^3}{12(1-\nu_m^2)}$ and ω_l is the dimensional natural frequency. The rapid convergence rate of the frequency parameter can be observed in Fig. 3 which verifies the numerical effectiveness of the proposed FE analysis. It can be also seen that the thin ($R/h = 50$) and moderately thick ($R/h = 20$) shells have completely different convergence patterns. This is due to the fact that the shells have different fundamental mode shapes where the thin shell has the axisymmetric deformation state while the moderately thick shell has the asymmetric one. After proving the accuracy and efficiency of the study, the parametric study is provided next.

In this study, the nonlinear vibration response is reported as the variation of the nonlinear frequency ratio which is the nonlinear to linear frequency ratio versus the non-dimensional deflection which is the maximum non-dimensional radial deflection ($\bar{v}_z^{max} = v_z^{max}/h$).

As the first example, given results in Table 4 are the linear frequency parameters and nonlinear frequency ratios versus the non-dimensional deflection for a fully hinged FGNC spherical shell with various RTRs (R/h) and weight fractions (W^*_{gpl}) and different distribution patterns of GPLs. The meridional angles are $\phi_0 = 30^\circ, \phi_1 = 120^\circ$. It is found that the shell with a higher weight fraction of GPLs and RTR has a higher frequency parameter while the FG-O type nanocomposite shell has the lowest frequency parameter.

Moreover, the large-amplitude vibration responses of the FGNC spherical shell for different RTRs and boundary supports are depicted in Fig. 4. The meridional angles are $\phi_0 = 30^\circ, \phi_1 = 90^\circ$ while the U-D nanocomposite shell

Table 3 Comparison study for the non-dimensional frequencies of the hinged FGNC spherical shell reinforced with CNTs

V_{cnt}^*		mode 1		mode 2		mode 3	
		Ansari *et al.* (2016)	Present work	Ansari *et al.* (2016)	Present work	Ansari *et al.* (2016)	Present work
0.12	U-D	179.9	179.8	183.5	183.4	193.0	192.8
	FG-A	174.9	174.8	175.5	175.4	188.4	188.2
	FG-O	166.0	166.0	169.2	169.2	178.8	178.7
	FG-X	192.3	192.1	196.3	196.0	197.2	197.0
0.17	U-D	227.6	227.4	232.1	232.0	244.2	244.0
	FG-A	222.7	222.5	223.4	223.2	240.0	238.8
	FG-O	211.9	211.8	216.1	216.0	228.4	228.1
	FG-X	243.1	242.8	248.2	248.0	255.9	255.6
0.28	U-D	252.3	252.1	257.3	257.1	266.2	266.0
	FG-A	247.0	246.8	248.4	248.2	265.5	265.3
	FG-O	234.1	234.0	238.4	238.3	252.0	251.8
	FG-X	273.5	273.2	275.2	274.9	281.2	279.9

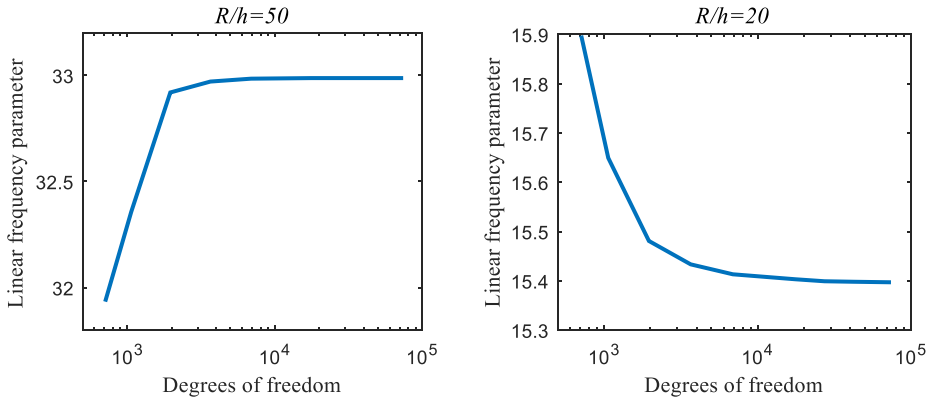

Fig. 3 Convergence study for the frequency parameters of FGNC spherical shell with Fixed-Fixed boundary supports ($\varphi_0 = 30°, \varphi_1 = 90°, W_{gpl}^* = 1\%$, FG-X)

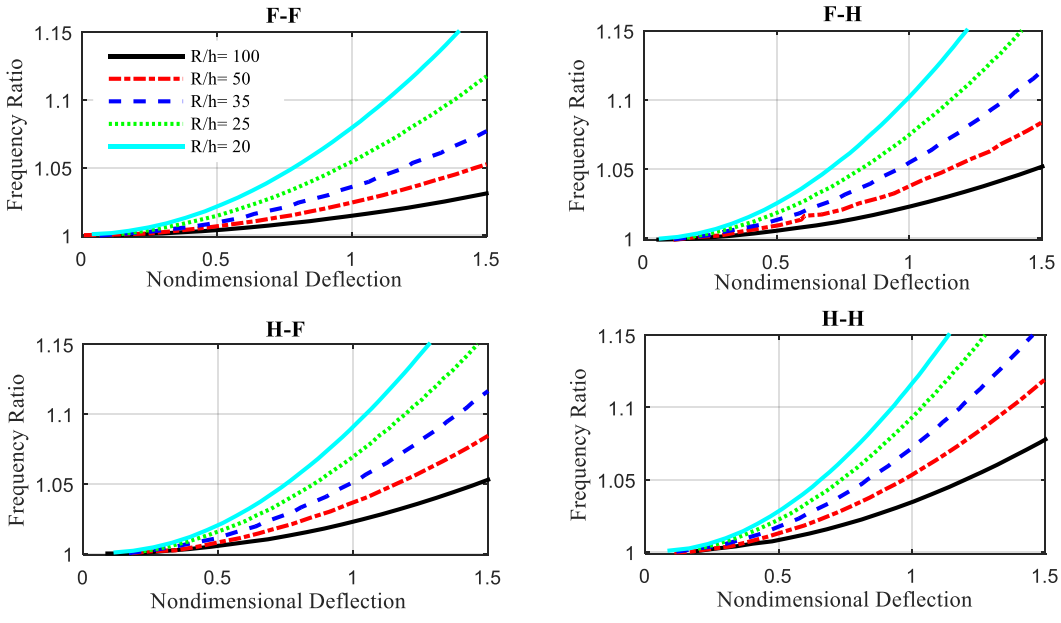

Fig. 4 Nonlinear vibration responses of the FGNC spherical shell for different radius to thickness ratios and boundary supports ($\varphi_0 = 30^\circ, \varphi_1 = 90^\circ, W_{gpl}^* = 1\%$, U-D)

Table 4 Linear frequency parameters and nonlinear frequency ratios for fully hinged FGNC spherical shell for different radius to thickness ratios (R/h) and weight fractions (W^*_{gpl}) for different distribution patterns of GPLs

R/h	W^*_{gpl}(%)		$\bar{\omega}_l$	v_z^{max}/h				
				0.2	0.4	0.6	0.8	1.0
100	0.5	U-D	36.43	1.0026	1.0074	1.0153	1.0263	1.0402
		FG-A	35.91	1.0022	1.0058	1.0118	1.0201	1.0307
		FG-O	36.29	1.0032	1.0096	1.0202	1.0349	1.0534
		FG-X	36.55	1.0023	1.0062	1.0127	1.0216	1.0329
	1.2	U-D	49.91	1.0025	1.0071	1.0147	1.0252	1.0385
		FG-A	48.63	1.0021	1.0056	1.0116	1.0202	1.0312
		FG-O	49.66	1.0035	1.0111	1.0234	1.0405	1.0620
		FG-X	50.13	1.0022	1.0055	1.0120	1.0217	1.0331
35	0.5	U-D	10.87	1.0044	1.0146	1.0312	1.0539	1.0821
		FG-A	10.49	1.0037	1.0117	1.0249	1.0429	1.0656
		FG-O	10.77	1.0052	1.0175	1.0377	1.0651	1.0991
		FG-X	10.96	1.0039	1.0125	1.0266	1.0458	1.0699
	1.2	U-D	14.90	1.0044	1.0146	1.0311	1.0537	1.0819
		FG-A	14.17	1.0035	1.0111	1.0234	1.0402	1.0615
		FG-O	14.72	1.0057	1.0195	1.0419	1.0723	1.1099
		FG-X	15.05	1.0037	1.0119	1.0252	1.0434	1.0663

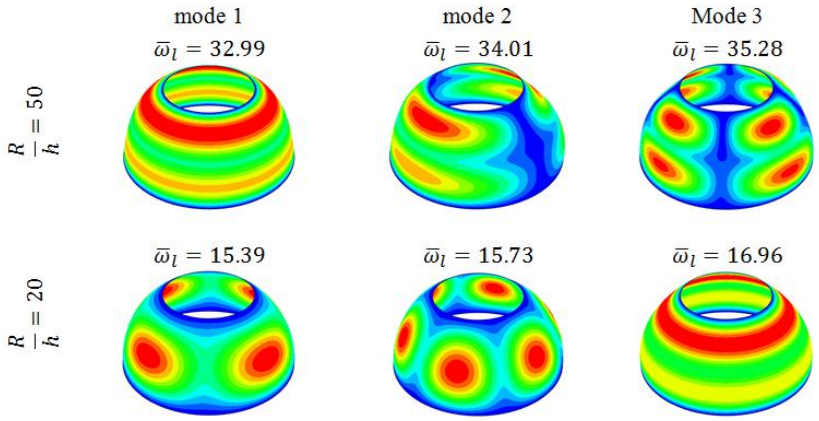

Fig. 5 The first three vibrational mode shapes of the fixed-fixed FGNC spherical shell for different radius to thickness ratios ($\varphi_0 = 30°, \varphi_1 = 90°, W^*_{gpl} = 1\%$, FG-X)

with $W^*_{gpl} = 1\%$ is considered. The results reveal that the thicker the FGNC shell is, the lower the frequency ratio is.

The same trend is concluded for all boundary supports. To highlight more insights into the impact of RTR on the vibrational behavior of FGNC spherical shells, Fig. 5 illustrates the first three modes shapes for two different thickness ratios and the most important observation here is that for some geometrical factors (here for $R/h = 20$) the fundamental mode shape is asymmetric so that the axisymmetric formulation can no longer be employed and the full asymmetric formulation should be utilized.

Nonlinear vibration responses of the fixed-fixed FGNC spherical shell are demonstrated in Fig. 6 for distinct meridional angles (φ_0) and distribution patterns of GPLs. The geometrical factors are: $\varphi_1 = 120^{\circ}, h/R = 0.02$ where the GPLs' weight fraction is 1.2%. The linear frequency parameters are also reported in Table 5 for various geometrical and material parameters as well as boundary supports where the specified factors are $h/R = 0.02$, $\varphi_1 = 120°$.

In addition, to give more details, the effects of large meridional angle (φ_1) on the first three mode shapes are shown in Fig. 7 for the U-D pattern and $\varphi_0 = 30$, $R/h = 50$, $W^*_{gpl} = 1\%$. It is noticed that the shell with the larger meridional length (with more differences between φ_0 and φ_1) has a smaller linear frequency parameter and larger nonlinear frequency ratio. This is due that by having a larger meridional length, the shell is more flexible with larger deformation and smaller frequency. Once again, it can be seen that in some cases the shell experiences the asymmetric fundamental mode shape that is $\varphi_1 = 60°$ in Fig. 7. As expected, The fixed-fixed (F-F) edge supports

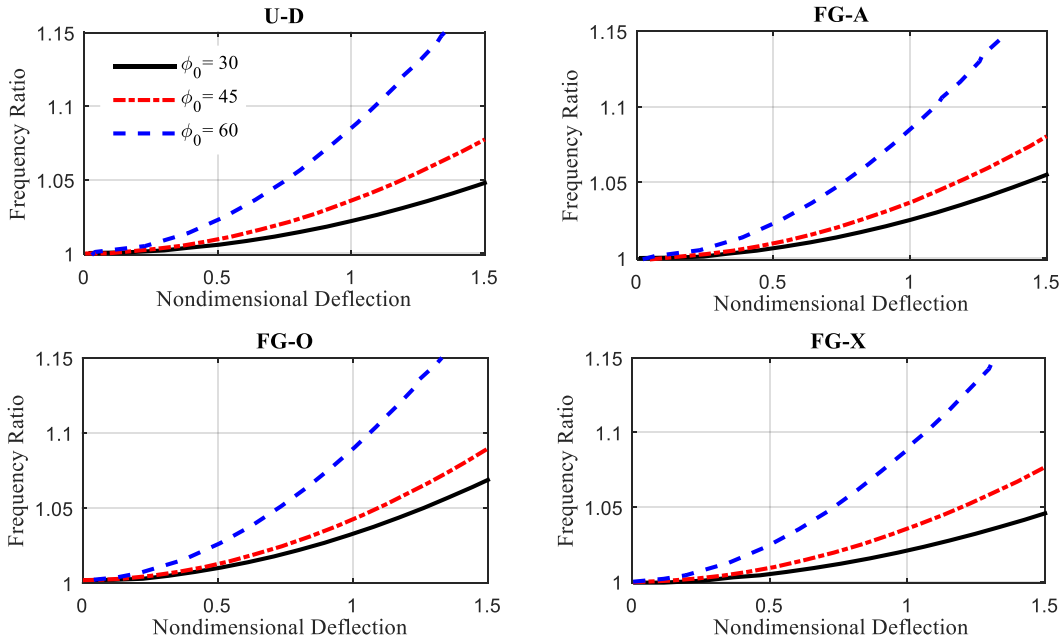

Fig. 6 Nonlinear vibration responses of the fixed-fixed FGNC spherical shell for different meridional angles (φ_0) and distribution patterns of GPLs ($\phi_1 = 120^{\circ}, h/R = 0.02, w^*_{gpl} = 1.2\%$)

Table 5 Linear frequency parameters of the FGNC spherical shell for different boundary supports

φ_0	$W^*_{gpl}(\%)$		F-F	F-H	H-F	H-H
30	0.5	U-D	19.679	19.092	19.138	18.574
		FG-A	19.560	18.772	18.849	18.082
		FG-O	19.456	18.928	18.970	18.462
		FG-X	19.863	19.230	19.278	18.670
	1	U-D	25.089	24.345	24.403	23.685
		FG-A	24.869	23.802	23.915	22.868
		FG-O	24.730	24.082	24.135	23.507
		FG-X	25.379	24.560	24.622	23.836
35	0.5	U-D	25.290	24.494	24.494	23.800
		FG-A	25.037	24.147	24.147	23.334
		FG-O	24.832	24.179	24.179	23.590
		FG-X	25.726	24.792	24.792	23.997
	1	U-D	32.244	31.229	31.229	30.345
		FG-A	31.778	30.631	30.631	29.565
		FG-O	31.521	30.732	30.732	30.015
		FG-X	32.928	31.698	31.698	30.657

give the highest frequency parameter, however, the point is that the maximum effect of constraints at boundaries is less than 7%.

The impacts of GPL's weight fraction on the large-amplitude vibration response of the fully fixed FGNC spherical shell are investigated in Fig. 8 for two RTRs. The FG-A pattern of nanocomposite spherical shell with $\varphi_0 = 45^{\circ}, \varphi_1 = 120^{\circ}$ is considered. Although the increase in GPL's weight fraction showed a significant increase in the linear frequency parameter in Tables 4 and 5, the results in Fig. 8 indicate that increasing the W^*_{gpl} has no remarkable influence on the nonlinear vibration response.

Demonstrated in Fig. 9 are the nonlinear vibration responses of the FGNC spherical shell for different GPL's dispersion patterns and meridional angles (φ_0). The geometrical and material-related factors are: $\varphi_1 = 120^{\circ}, R/h = 100, W^*_{gpl} = 1\%$. Although quite close results are given for the small deflections (let us say $v_z^{max}/h < 1$) for distinct GPL patterns, considerable differences in nonlinear responses are found for larger deflections, while the results in Table 5 revealed that the GPLs dispersion patterns do not have a substantial impact on the linear frequency parameter.

The effects of boundary support on the nonlinear

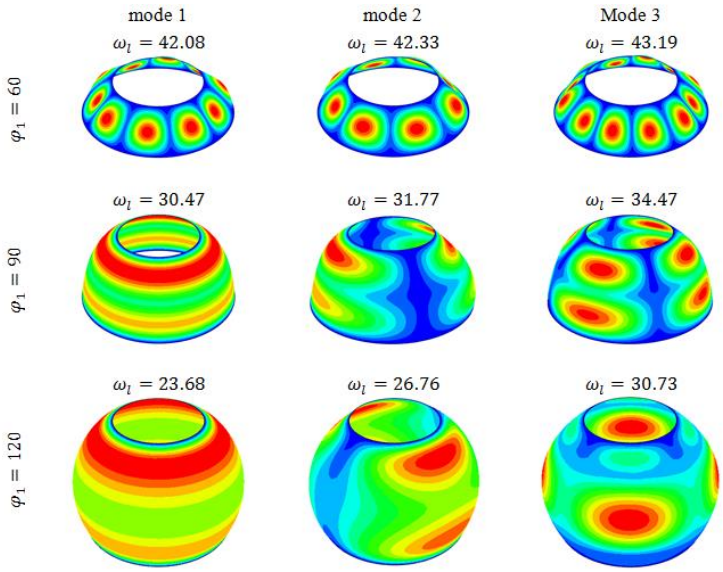

Fig. 7 The first three vibrational mode shapes of the hinged-hinged FGNC spherical shell for different meridional angles

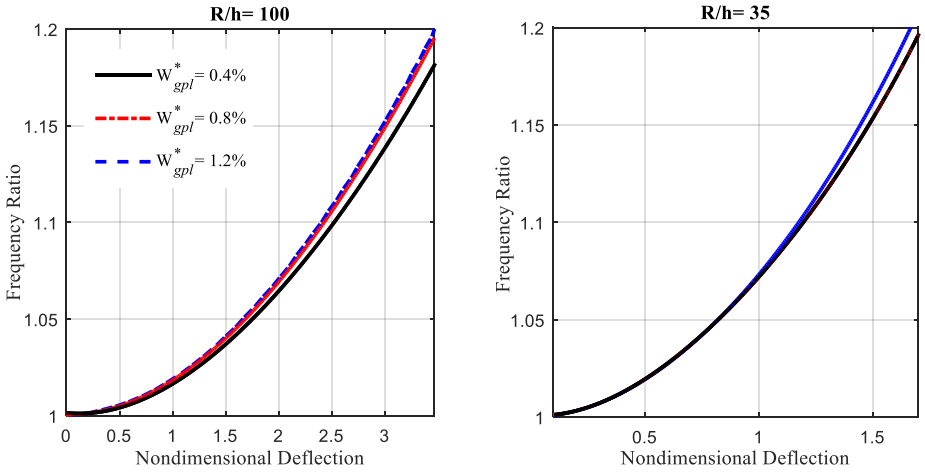

Fig. 8 Nonlinear vibration responses of the fixed-fixed FGNC spherical shell for different GPLs weight fractions and radius to thickness ratios

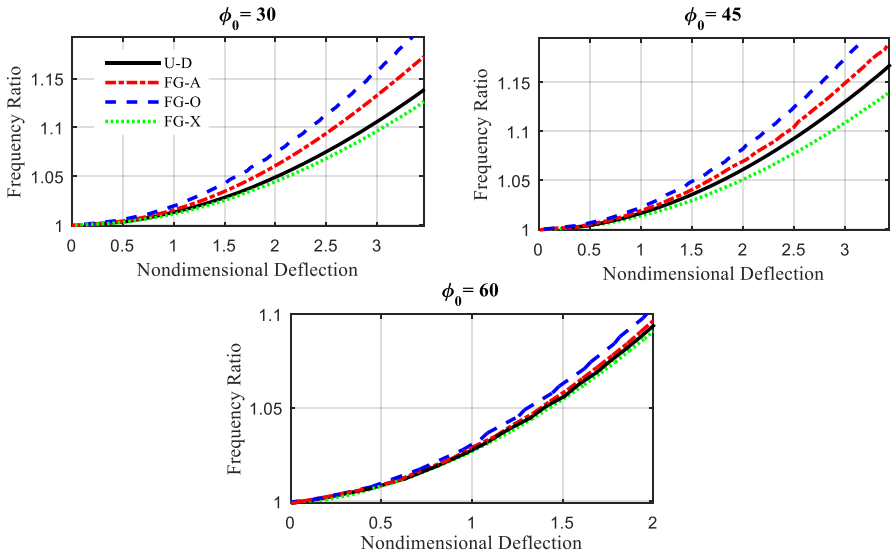

Fig. 9 Nonlinear vibration responses of the fixed-fixed FGNC spherical shell for different GPLs distribution patterns and meridional angles

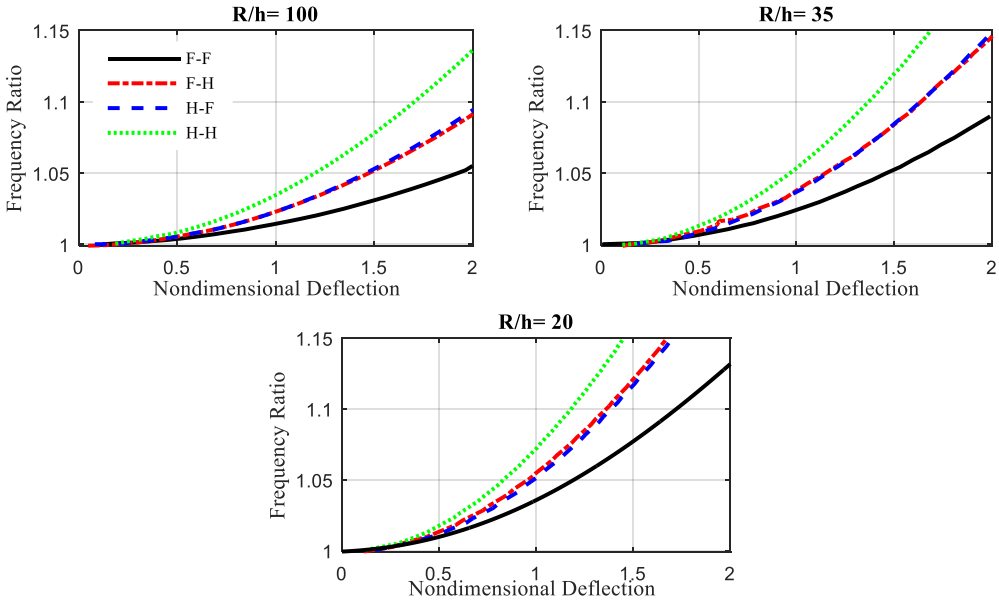

Fig. 10 Nonlinear vibration responses of the FGNC spherical shell for different boundary supports and radius to thickness ratios

vibration response of the FGNC spherical shells are demonstrated in Figure 10 for three thickness ratios (i.e., $R/h = 100,35,20$). The meridional angles are $\varphi_0 = 30^{\circ}, \varphi_1 = 90^{\circ}$ where the U-D pattern with $W^*_{gpl} = 1\%$ is regarded. It is apparent that the hinged-hinged (H-H) shell has the highest frequency ratio while the fixed-hinged (F-H) and hinged-fixed (H-F) shells have quite close responses (almost the same) and the fully fixed supports (F-F) leads to the lowest nonlinear frequency ratio. The results also express that the impact of boundary support is more important for a thicker shell than a thinner one.

6. Conclusions

The nonlinear finite element analysis was implemented to study the effects of geometrically nonlinear assumptions on the vibration of nanocomposite spherical shells reinforced with functionally graded GPLs. The shear deformation shell theory along with the von Kármán nonlinear kinematic relations with asymmetric deformation state was applied to derive the fundamental mathematical formulations and energy functional using Hamilton's principle. The extended Halpin-Tsai model is utilized to specify the overall Young's modulus of the nanocomposite. Then, the eight-node shell element in spherical coordinate was implemented for FE discretization and the Harmonic balance method with the Newton-Raphson iterative technique was employed to find the nonlinear dynamic response. The correctness and performance of the proposed numerical model were first verified through various comparative and convergence studies and then the impacts of involved factors on the nonlinear dynamics of FGNC spherical shells were analyzed. The main conclusion is that in some cases with specific geometrical parameters (moderately thick shells or shells with short meridional length), the spherical shell had the asymmetric fundamental vibrational mode so that the axisymmetric formulation could not be appropriately used to model the problem and the implementation of the asymmetric formulation was inevitable. It was also figured out that the FGNC shells with FG-X and FG-O dispersion patterns have the lowest and highest nonlinear frequency ratios while no significant effect on the linear frequency parameter was observed. Increasing the GPLs weight fraction remarkably enhanced the linear frequency parameters, however, had an insignificant effect on the nonlinear frequency ratio.

Acknowledgment

This work was supported by Natural Science Foundation of Chongqing Province (General Program): cstc2020jcyj-msxmX0050 (Preparation technology and performance optimization of nanocrystalline high-entropy alloy based on molecular dynamics).

References

Ansari, R., Torabi, J. and Shojaei, M.F. (2016), "Vibrational analysis of functionally graded carbon nanotube-reinforced composite spherical shells resting on elastic foundation using the variational differential quadrature method", *Eur. J. Mech. A Solids*, **60**, 166-182. https://doi.org/10.1016/j.euromechsol.2016.07.003.

Ansari, R., Hasrati, E. and Torabi, J. (2020), "Effect of external pressure on the vibration analysis of higher order shear deformable FG-CNTRC spherical panels", *Eng. Comput.*, **38**, 43-54. https://doi.org/10.1007/s00366-020-01138-0.

Civalek, Ö. (2020), "Vibration of functionally graded carbon nanotube reinforced quadrilateral plates using geometric transformation discrete singular convolution method", *Int. J.*

Numer. Meth. Eng., **121**(5), 990-1019. https://doi.org/10.1002/nme.6254.

Ebrahimi, F. and Habibi, S. (2017), "Low-velocity impact response of laminated FG-CNT reinforced composite plates in thermal environment", *Adv. Nano Res.*, **5**(2), 69. https://doi.org/10.12989/anr.2017.5.2.069.

Fantuzzi, N., Tornabene, F., and Viola, E. (2014), "Generalized differential quadrature finite element method for vibration analysis of arbitrarily shaped membranes", *Int. J. Mech. Sci.*, **79**, 216-251. https://doi.org/10.1016/j.ijmecsci.2013.12.008.

Gao, K., Gao, W., Chen, D. and Yang, J. (2018), "Nonlinear free vibration of functionally graded graphene platelets reinforced porous nanocomposite plates resting on elastic foundation", *Compos. Struct.*, **204**, 831-846. https://doi.org/10.1016/j.compstruct.2018.08.013.

Gholami, R. and Ansari, R. (2018), "Nonlinear harmonically excited vibration of third-order shear deformable functionally graded graphene platelet-reinforced composite rectangular plates", *Eng. Struct.*, **156**, 197-209. https://doi.org/10.1016/j.engstruct.2017.11.019.

Haboussi, M., Sankar, A. and Ganapathi, M. (2021), "Nonlinear axisymmetric dynamic buckling of functionally graded graphene reinforced porous nanocomposite spherical caps", *Mech. Adv. Mater. Struct.*, **28**(2), 127-140. https://doi.org/10.1080/15376494.2018.1549296.

Hajmohammad, M.H., Zarei, M.S., Farrokhian, A. and Kolahchi, R. (2018), "A layerwise theory for buckling analysis of truncated conical shells reinforced by CNTs and carbon fibers integrated with piezoelectric layers in hygrothermal environment", *Adv. Nano Res.*, **6**(4), 299. https://doi.org/10.12989/anr.2018.6.4.299.

Heydarpour, Y., Malekzadeh, P., Dimitri, R. and Tornabene, F. (2020), "Thermoelastic analysis of rotating multilayer FG-GPLRC truncated conical shells based on a coupled TDQM-NURBS scheme" *Compos. Struct.*, **235**, 111707. https://doi.org/10.1016/j.compstruct.2019.111707.

Khadir, A.I., Daikh, A.A. and Eltaher, M.A. (2021), "Novel four-unknowns quasi 3D theory for bending, buckling and free vibration of functionally graded carbon nanotubes reinforced composite laminated nanoplates", *Adv. Nano Res.*, **11**(6), 621-640. https://doi.org/10.12989/anr.2021.11.6.621.

Kiani, Y. (2017), "Free vibration of FG-CNT reinforced composite spherical shell panels using Gram-Schmidt shape functions", *Compos. Struct.*, **159**, 368-381. https://doi.org/10.1016/j.compstruct.2016.09.079.

Kiani, Y. (2019), "Buckling of functionally graded graphene reinforced conical shells under external pressure in thermal environment", *Compos. Part B Eng.*, **156**, 128-137. https://doi.org/10.1016/j.compositesb.2018.08.052.

Kiarasi, F., Babaei, M., Mollaei, S., Mohammadi, M. and Asemi, K. (2021), "Free vibration analysis of FG porous joined truncated conical-cylindrical shell reinforced by graphene platelets", *Adv. Nano Res.*, **11**(4), 361-380. https://doi.org/10.12989/anr.2021.11.4.361.

Krack, M. and Gross, J. (2019), *Harmonic Balance for Nonlinear Vibration Problems*, Springer, New York.

Kumar, Y., Gupta, A. and Tounsi, A. (2021), "Size-dependent vibration response of porous graded nanostructure with FEM and nonlocal continuum model", *Adv. Nano Res.*, **11**(1). https://doi.org/10.12989/anr.2021.11.1.001.

Liu, D., Kitipornchai, S., Chen, W. and Yang, J. (2018), "Three-dimensional buckling and free vibration analyses of initially stressed functionally graded graphene reinforced composite cylindrical shell", *Compos. Struct.*, **189**, 560-569. https://doi.org/10.1016/j.compstruct.2018.01.106.

Liu, D., Zhou, Y. and Zhu, J. (2021), "On the free vibration and bending analysis of functionally graded nanocomposite spherical shells reinforced with graphene nanoplatelets: Three-dimensional elasticity solutions", *Eng. Struct.*, **226**, 111376. https://doi.org/10.1016/j.engstruct.2020.111376.

Nejadi, M.M., Mohammadimehr, M. and Mehrabi, M. (2021), "Free vibration and buckling of functionally graded carbon nanotubes/graphene platelets Timoshenko sandwich beam resting on variable elastic foundation", *Adv. Nano Res.*, **10**(6), 539-548. https://doi.org/10.12989/anr.2021.10.6.539.

Noroozi, A.R., Malekzadeh, P., Dimitri, R. and Tornabene, F. (2020), "Meshfree radial point interpolation method for the vibration and buckling analysis of FG-GPLRC perforated plates under an in-plane loading", *Eng. Struct.*, **221**, 111000. https://doi.org/10.1016/j.engstruct.2020.111000.

Qin, Z., Zhao, S., Pang, X., Safaei, B. and Chu, F. (2020), "A unified solution for vibration analysis of laminated functionally graded shallow shells reinforced by graphene with general boundary conditions", *Int. J. Mech. Sci.*, **170**, 105341. https://doi.org/10.1016/j.ijmecsci.2019.105341

Qu, Y., Long, X., Yuan, G. and Meng, G. (2013), "A unified formulation for vibration analysis of functionally graded shells of revolution with arbitrary boundary conditions", *Compos. Part B Eng.*, **50**, 381-402. https://doi.org/10.1016/j.compositesb.2013.02.028.

Salami, S.J., Boroujerdy, M.S. and Bazzaz, E. (2021), "Geometrically nonlinear thermo-mechanical bending analysis of deep cylindrical composite panels reinforced by functionally graded CNTs", *Adv. Nano Res.*, **10**(4), 385-395. https://doi.org/10.12989/anr.2021.10.4.385.

Selim, B.A. and Liu, Z. (2021), "Impact analysis of functionally-graded graphene nanoplatelets-reinforced composite plates laying on Winkler-Pasternak elastic foundations applying a meshless approach", *Eng. Struct.*, **241**, 112453. https://doi.org/10.1016/j.engstruct.2021.112453.

Shen, H.S., Xiang, Y. and Lin, F. (2017a), "Nonlinear vibration of functionally graded graphene-reinforced composite laminated plates in thermal environments", *Comput. Meth. Appl. Mech. Eng.*, **319**, 175-193. https://doi.org/10.1016/j.cma.2017.02.029.

Shen, H.S., Xiang, Y., Lin, F. and Hui, D. (2017b), "Buckling and postbuckling of functionally graded graphene-reinforced composite laminated plates in thermal environments", *Compos. Part B Eng.*, **119**, 67-78. https://doi.org/10.1016/j.compositesb.2017.03.020.

Shen, H.S., Xiang, Y. and Fan, Y. (2017c), "Nonlinear vibration of functionally graded graphene-reinforced composite laminated cylindrical shells in thermal environments", *Compos. Struct.*, **182**, 447-456. https://doi.org/10.1016/j.compstruct.2017.09.010.

Sobhani, E. (2022), "Vibrational performance modeling for coupling of a full-ellipsoid shell with a cylindrical shell with a focus on flexibility at coupling and boundary conditions via the GDQ-meshless method", *Eng. Anal. Bound. Elem.*, **144**, 329-351. https://doi.org/10.1016/j.enganabound.2022.08.037.

Sobhani, E. and Avcar, M. (2022a), "The influence of various nanofiller materials (CNTs, GNPs, and GOPs) on the natural frequencies of Nanocomposite Cylindrical Shells: A comparative study", *Mater. Today Commun.*, **33**, 104547. https://doi.org/10.1016/j.mtcomm.2022.104547.

Sobhani, E. and Avcar, M. (2022b), "Natural frequency analysis of imperfect GNPRN conical shell, cylindrical shell, and annular plate structures resting on Winkler-Pasternak Foundations under arbitrary boundary conditions", *Eng. Anal. Bound. Elem.*, **144**, 145-164. https://doi.org/10.1016/j.enganabound.2022.08.018.

Sobhani, E. and Masoodi, A.R. (2022), "On the frequencies of graphene nanoplatelet agglomerated nanocomposite paired paraboloidal-cylindrical shells under arbitrary boundary conditions", *Aerosp. Sci. Technol.*, **128**, 107782. https://doi.org/10.1016/j.ast.2022.107782.

Sobhani, E., Masoodi, A.R. and Ahmadi-Pari, A.R. (2022a), "Free-damped vibration analysis of graphene nano-platelet nanocomposite joined conical-conical-cylindrical shell marine-like structures", *Ocean Eng*., **261**, 112163. https://doi.org/10.1016/j.oceaneng.2022.112163.

Sobhani, E., Masoodi, A.R. and Ahmadi-Pari, A.R. (2022b), "Circumferential vibration analysis of nano-porous-sandwich assembled spherical-cylindrical-conical shells under elastic boundary conditions", *Eng. Struct.*, **273**, 115094. https://doi.org/10.1016/j.engstruct.2022.115094.

Sobhani, E., Masoodi, A.R. and Ahmadi-Pari, A.R. (2022c), "Wave frequency responses estimate of the nanocomposite linked hemispherical-conical shell underwater-like bodies with the impacts of two types of graphene-based nanofillers", *Ocean Eng*., **262**, 112329. https://doi.org/10.1016/j.oceaneng.2022.112329.

Sobhani, E. (2023a), "Vibrational characteristics of fastening of a spherical shell with a coupled conical-conical shells strengthened with nanocomposite sandwiches contained agglomerated CNT face layers and GNP core under spring boundary conditions", *Eng. Anal. Bound. Elem*., **146**, 362-387. https://doi.org/10.1016/j.enganabound.2022.10.035.

Sobhani, E. (2023b), "Improvement of vibrational characteristics of multipurpose structures (plate and shells) used in aerospace components by deploying Graphene Oxide Powders (GOPs) in a matrix as a nano-reinforcement: A comprehensive study", *Eng. Anal. Bound. Elem*., **146**, 598-635. https://doi.org/10.1016/j.enganabound.2022.11.014.

Sobhani, E., Masoodi, A.R., Dimitri, R. and Tornabene, F. (2023), "Free vibration of porous graphene oxide powder nano-composites assembled paraboloidal-cylindrical shells", *Compos. Struct*., **304**, 116431. https://doi.org/10.1016/j.compstruct.2022.116431.

Song, M., Yang, J. and Kitipornchai, S. (2018), "Bending and buckling analyses of functionally graded polymer composite plates reinforced with graphene nanoplatelets", *Compos. Part B Eng*., **134**, 106-113. https://doi.org/10.1016/j.compositesb.2017.09.043.

Tao, C. and Dai, T. (2021), "Postbuckling of multilayer cylindrical and spherical shell panels reinforced with graphene platelet by isogeometric analysis", *Eng. Comput*. 1-16. https://doi.org/10.1007/s00366-021-01360-4.

Tornabene, F. and Viola, E. (2007), "Vibration analysis of spherical structural elements using the GDQ method", *Comput. Math. Appl*., **53**(10), 1538-1560. https://doi.org/10.1016/j.camwa.2006.03.039.

Tornabene, F., Liverani, A. and Caligiana, G. (2012), "General anisotropic doubly-curved shell theory: A differential quadrature solution for free vibrations of shells and panels of revolution with a free-form meridian", *J. Sound Vib*., **331** (22), 4848-4869. https://doi.org/10.1016/j.jsv.2012.05.036.

Van Do, V.N. and Lee, C.H. (2020), "Static bending and free vibration analysis of multilayered composite cylindrical and spherical panels reinforced with graphene platelets by using isogeometric analysis method", *Eng. Struct.*, **215**, 110682. https://doi.org/10.1016/j.engstruct.2020.110682.

Wang, Q., Pang, F., Qin, B. and Liang, Q. (2018), "A unified formulation for free vibration of functionally graded carbon nanotube reinforced composite spherical panels and shells of revolution with general elastic restraints by means of the Rayleigh-Ritz method", *Polym. Compos*., **39**(S2), E924-E944. https://doi.org/10.1002/pc.24339.

Wang, A., Pang, Y., Zhang, W. and Jiang, P. (2019), "Nonlinear dynamic analysis of functionally graded graphene reinforced composite truncated conical shells", *Int. J. Bifurc. Chaos*, **29**(11), 1950148. https://doi.org/10.1142/S0218127419501487.

Yang, J., Chen, D. and Kitipornchai, S. (2018), "Buckling and free vibration analyses of functionally graded graphene reinforced porous nanocomposite plates based on Chebyshev-Ritz method", *Compos. Struct*., **193**, 281-294. https://doi.org/10.1016/j.compstruct.2018.03.090.

Zhao, S., Zhao, Z., Yang, Z., Ke, L., Kitipornchai, S. and Yang, J. (2020), "Functionally graded graphene reinforced composite structures: A review", *Eng. Struct*., **210**, 110339. https://doi.org/10.1016/j.engstruct.2020.110339.

AT